Local and global chromatin interactions are altered by large genomic deletions associated with human brain development

Ying Zhang[1*], Xianglong Zhang[2,3*], Xiaowei Zhu[2,3*], Carolin Purmann[2,3], Michael S Haney[3], Thomas Ward[2,3], Jie Yao[4], Sherman M Weissman[5#], Alexander E Urban[2,3#]

1 Department of Genetics and Genomic Sciences, Icahn School of medicine at Mount Sinai, 2 Department of Psychiatry and Behavioral Sciences, 3 Department of Genetics, Stanford University School of Medicine, 4 Department of Cell Biology, Yale University School of Medicine, 5 Department of Genetics, Yale University

Email addresses:

Ying Zhang, zzhang006@gmail.com;

Xianglong Zhang, xzhang8@stanford.edu;

Xiaowei Zhu, xwzhu@stanford.edu;

Carolin Purmann, purmann@stanford.edu;

Michael S Haney, haney@stanford.edu;

Thomas Ward, wardtr@stanford.edu;

Jie Yao, yao.j@yale.edu;

Sherman M Weissman, sherman.weissman@yale.edu;

Alexander E Urban, aeurban@stanford.edu.

*These authors contributed equally to this work.

#To whom correspondence should be addressed.

Abstract

Background: Large copy number variants (CNVs) in the human genome are strongly associated with common neurodevelopmental, neuropsychiatric disorders such as schizophrenia and autism. Using Hi-C analysis of long-range chromosome interactions and ChIP-Seq analysis of regulatory histone marks we studied the epigenomic effects of the prominent large deletion CNV on chromosome 22q11.2 and also replicated a subset of the findings for the large deletion CNV on chromosome 1q21.1.

Results: We found that, in addition to local and global gene expression changes, there are pronounced and multilayered effects on chromatin states, chromosome folding and topological domains of the chromatin, that emanate from the large CNV locus. Regulatory histone marks are altered in the deletion proximal regions, and in opposing directions for activating and repressing marks. There are also significant changes of histone marks elsewhere along chromosome 22q and genome wide. Chromosome interaction patterns are weakened within the deletion boundaries and strengthened between the deletion proximal regions. We detected a change in the manner in which chromosome 22q folds onto itself, namely by increasing the long-range contacts between the telomeric end and the deletion proximal region. Further, the large CNV affects the topological domain that is spanning its genomic region. Finally, there is a widespread and complex effect on chromosome interactions genome-wide, i.e. involving all other autosomes, with some of the effect directly tied to the deletion region on 22q11.2.

Conclusions: These findings suggest novel principles of how such large genomic deletions can alter nuclear organization and affect genomic molecular activity.

Keywords: Germline CNVs, Chromatin States, Chromosome Interactions, Topological Domains

Introduction

Two of the most exciting discoveries in human genetics of the past decade are that small- to medium-sized Copy Number Variants (CNVs) are very common in the human genome, and that there is a group of large CNVs that are strongly associated with brain development and neuropsychiatric disorders such as schizophrenia and the autism spectrum disorders (ASDs) [1,2]. These large CNVs are understood to be providing enticing points of entry to the analysis of the strong but complex genetic and molecular (and possibly even cellular) basis of these common disorders.

We now know that small to medium-sized CNVs, i.e. deletions or duplications of genomic DNA sequence ranging in size from hundreds to tens of thousands of basepairs, are present in any human genome with their numbers in the thousands [3-7]. Not very much is known as of yet about such smaller CNVs' effects on the normal phenotype, but some examples already exist that show that such effects could be considerable, such as the copy number variation of the amylase gene associated with a given human population's ability to digest high-starch food [8].

Large CNVs, typically sized from hundreds of thousands to millions of basepairs of genomic DNA sequence, were previously known to be in strong association with often-severe but rare congenital malformations, or found in cancer genomes. It was a striking discovery when a series of studies [1,2] showed that there is a group of more than ten large CNVs that are strongly associated with aberrant brain development and a resulting neuropsychiatric phenotype such as schizophrenia, ASD or Williams Syndrome. These large

68 neuropsychiatric CNVs can encompass many genes and their effects across the various
69 molecular levels of gene activity and regulation and the clinical phenotype are complex and
70 only poorly understood.

71 On the molecular level these large neuropsychiatric CNVs have been mostly studied by
72 applying the research paradigm of trying to determine which single gene from within the
73 CNV boundaries is at the root of the large CNV's effects on brain development. Many very
74 interesting insights have been gained using this approach into a considerable number of
75 genes with these large CNVs.

76 However, these insights about individual genes fall far short of explaining the full
77 effects of the large CNVs. Also there already have been a number of transcriptome wide
78 studies that at least hint at certain network effects emanating from the large CNVs. Which
79 mechanisms mediate such transcription network effects is then the question. Furthermore
80 there are an increasing number of studies that show a potentially very important role of
81 chromatin regulation in the molecular etiology of neuropsychiatric disorder [9-15].

82 Against this backdrop we reasoned that it was worthwhile testing whether large CNVs
83 with association to brain development might cause a disruption or at least alteration of one
84 or several aspects of chromatin conformation, such as the distribution of regulatory
85 chromatin marks, the long-range direct physical interactions between distant regions on
86 one chromosome or between different chromosomes or the higher-order chromatin domain
87 structures that are defined by such marks or interactions. Such effects on these important
88 layers of molecular regulation of gene activity would then constitute a novel principle by
89 which large CNVs could transmit their presence to the machinery of cellular physiology.

Here we show in a cohort of cell lines derived from patients with 22q11 Deletion Syndrome that indeed chromatin marks, chromatin domains and long-range chromosome interactions are affected in several distinct ways by a large, common and disease-associated CNV on chromosome 22q11.2. We then go on to show in a smaller set of cell lines from different patients that at least some of the same observations can also be made with another neuropsychiatric large CNV, on chromosome 1q21.1.

22q11 Deletion Syndrome (22q11DS) is a disorder caused by a heterozygous deletion of 3 million basepairs containing more than 60 known genes on chromosome 22q11.2. It occurs in at least 1 in 4,000 live births. The common phenotypes of 22q11DS include a large spectrum of congenital anomalies, for example of the facial structures and the cardiovascular system – and notably there is a strong association with several neurodevelopmental psychiatric disorders, in particular schizophrenia and ASDs [2,16-19]. In this study we are using the large CNV on 22q11.2 as a model to determine the generalizable principles along which large CNVs of this important category can lead to changes to the various ways in which chromatin is ordered, using unbiased, genome-wide, sequencing-based assays for discovery.

Results

High-volume sequencing data generation for Hi-C chromosomal contact maps, ChIP-Seq chromatin marks and RNA-Seq gene expression data

To determine possible effects of the 22q11.2 deletion on chromosomal interactions, we generated Hi-C contact maps for 11 human lymphoblastoid cell lines (5 patient cell lines with 22q11.2 deletion and 6 control cell lines without), with a total of 3.1 billion Hi-C contact-reads of which 680 million read-pairs were of high quality and used for the

113 downstream analyses (**Supplementary Table 1**). The existence of the 3 Mbp deletion in the
114 patient cell lines was validated by whole genome sequencing **(Supplementary Fig. 1)**.

115 As a first means of quality control we included in our data generation and analysis the
116 cell line GM06990, which was the cell line used in the original Hi-C paper [20].
117 Interchromosomal contacts of GM06990 as determined by our own Hi-C data for this line
118 (**Supplementary Fig. 2a**) show the same patterns of chromosomal interactions across the
119 nucleus as in [20]; i.e. small chromosomes generally have more interactions with each other
120 than larger chromosomes with each other, and many more than chromosomes in the
121 medium size range. Specific interaction pairs, e.g. between chromosomes 17 and 19 were
122 also replicated in our GM06990 data. Global interchromosomal contact maps resulting from
123 combining all our controls and cases, respectively, again replicated these global interaction
124 patterns (**Supplementary Fig. 2b,c**).

125 To determine the effects of 22q11.2 deletion on gene expression patterns and
126 chromatin marks we performed RNA-Seq on 14 cell lines (**Supplementary Table 1**) and
127 ChIP-seq of H3K27ac and H3K27me3 for 6 cell lines and CTCF for 5 of the same cell lines,
128 respectively (**Supplementary Table 2**).

129 **Normalization of Hi-C data**

130 Many factors, such as mappability of sequencing reads, GC content, length of the restriction
131 enzyme fragment etc., can lead to biases in Hi-C data. Several alternative computational
132 approaches have been developed for the normalization of Hi-C data with the aim to remove
133 these biases [21-30]. While these approaches use different algorithmic principles, it has been
134 demonstrated that when using them on Hi-C data generated for control genomes without
135 large CNVs, such as GM12878, the normalization metrics will be highly correlated across the

various normalization schemes [31]. For our Hi-C data however, we needed to be certain to use a normalization method that is not thrown off from the outset by the presence of the heterozygous 3 Mbp deletion in 22q11.2.

We tested three commonly used different normalization algorithms that were developed for Hi-C data, using the rationale that the normalization methods should not change the general patterns of interaction we can see in the raw data.

We found that not all of the available normalization methods are robust for use with Hi-C data coming from genomes with large CNVs but that the hicpipe algorithm [21] is quite suitable for this purpose (details of the comparison between normalization methods in the **Supplementary Information** and **Supplementary Fig. 3**).

Chromosomal contacts decrease within the 22q11.2 deletion boundaries and between the deletion region and the remainder of chromosome 22q

We observed that the chromosomal contacts within the 22q11.2 deletion regions in 22q11DS lines decreased significantly compared to control cell lines (**Fig. 1a**). Also strongly reduced in the deletion cell lines were the chromosomal contacts between the 22q11.2 deletion region with the entire remainder of chromosome 22 (**Fig. 1a; Supplementary Fig. 4a**). This dosage effect is consistent with the copy number of the 22q11.2 deletion region in the patient cell lines, as all of the 22q11DS cell lines are heterozygously deleted for this region. No such dosage effect on the chromosomal contacts was observed that did not involve the 22q11.2 region. Furthermore, there was no such strong dosage effect on intrachromosomal contacts on any of the other autosomes (for example chromosome 19 in **Fig. 1b; Supplementary Fig. 4b**).

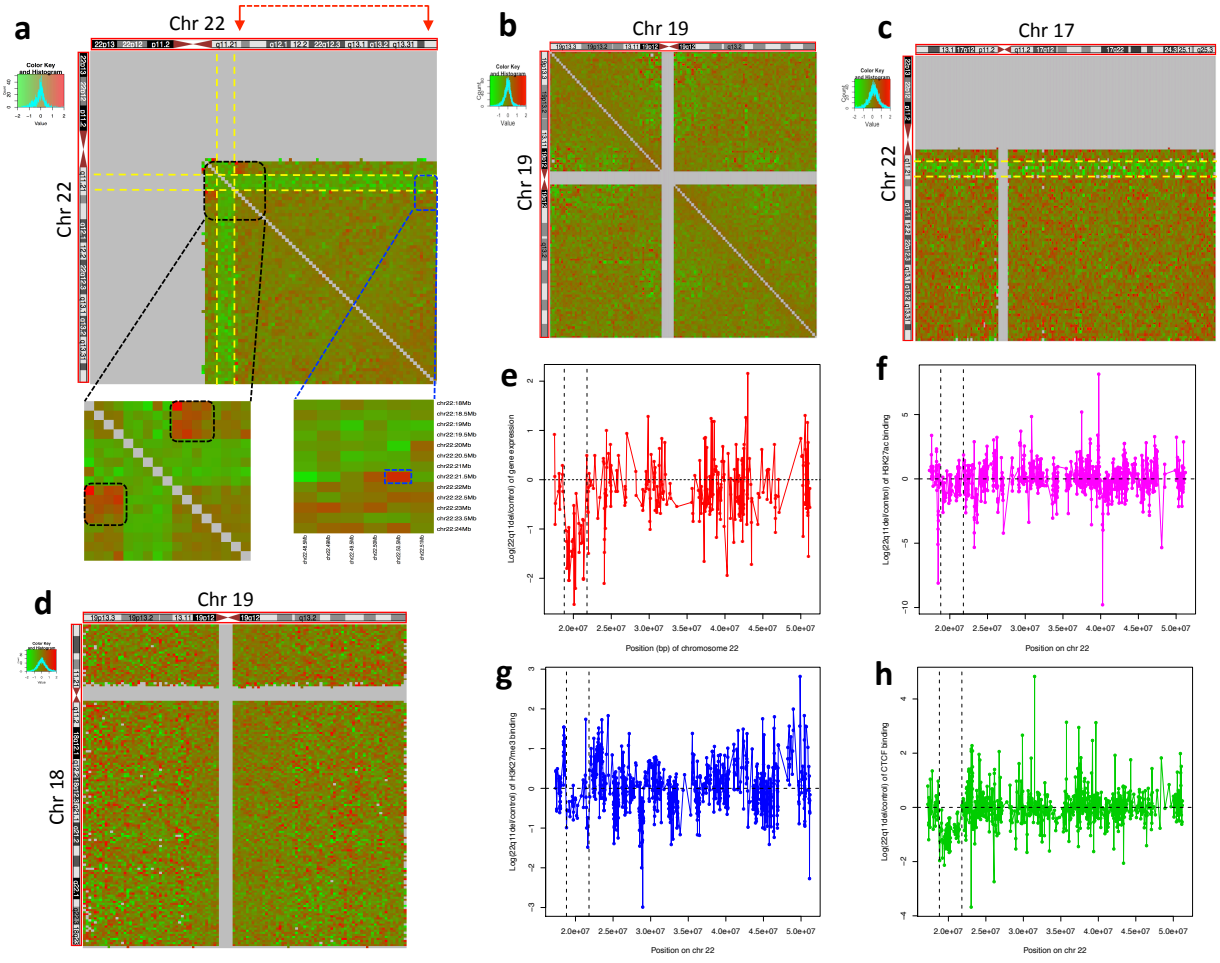

Figure 1. Effects of the 22q11.2 deletion on chromosome contacts, gene expression and epigenetic profiles. *Panels a-d: each pixel in the heat-maps represents the intra- or inter-chromosomal contact frequency in Hi-C data from 22q11.2del cell lines versus control cell lines for a 500 kbp region. Yellow dashed lines indicate the 3 Mbp deletion on chromosome 22q. (a) Fold change of cis-contacts along chromosome 22 in 22q11.2del versus control cell lines. Black boxes indicate increased contacts between the deletion-flanking regions in 22q11.2del cell lines. Blue box: the signal for increased contacts between the downstream deletion-flanking region and the telomeric end of chromosome 22q (red arrows and dashed red line indicate the corresponding chromosome folding event). (b) Lack of intra-chromosomal fold change of contacts for chromosome 19. (c) Fold change of inter-chromosomal contacts between*

chromosome 22 and chromosome 17. (d) Lack of intra-chromosomal fold change of contacts between chromosome 18 and chromosome 19. (e) Log2 transformed fold change of gene expression for genes on chromosome 22q in RNA-Seq data from 22q11.2del versus cell lines. Each point represents a gene. Panels f-h: Log2 transformed fold change in ChIP-Seq signals in 22q11.2del versus control cell lines. (f) H3K27ac histone modifications. (g) H3K27me3 histone modifications. (h) CTCF binding sites. Black dashed lines indicate the 3 Mbp deletion on chromosome 22q in e-h.

Then we investigated whether this dosage effect of the 22q11.2 deletion on *cis*-contacts (i.e. within the deletion boundaries and between the deletion region and elsewhere on chromosome 22q) holds for *trans*-contacts as well (i.e. for contacts between the region within the deletion boundaries and the rest of the genome). We found the *trans*-contacts involving the 22q11.2 deletion in the patient cell lines and any other chromosome also decreased compared to control cell lines (**Fig. 1c; Supplementary Fig. 4c**). No other regions of chromosome 22q showed such an effect, and neither did any other pair of autosomes that did not include 22q (**Fig. 1d; Supplementary Fig. 4d**).

The 22q11.2 deletion has an effect on gene expression and epigenetic profiles in the 22q11.2 region

Next we set out to identify the effects of the 22q11.2 deletion on gene expression and epigenetic profiles. RNA-Seq analysis showed that all of the genes that were expressed within the deletion boundaries in the 22q11.2 region showed decreased expression in 22q11.2DS patient lines relative to control cell lines (**Fig. 1e**). Our findings are consistent with a previous study [32].

Differential pattern analysis of H3K27ac, H3K27me3 and CTCF by ChIP-Seq showed the

majority of binding sites for these essential chromatin marks within the 22q11.2 deletion boundaries with decreased signals in 22q11.2DS patient lines compared to control cell lines (**Fig. 1f,g,h**). These decreased binding signals for such a large region are specific to chromosome 22q11.

Chromosome contacts increase across the 22q11DS breakpoint junction and chromatin marks in its flanking regions are affected in a concerted manner

The flanking regions upstream and downstream of the 22q11.2 deletion are brought into close proximity to each other by the formation of the deletion breakpoint junction. We hypothesized that since Hi-C contacts between two given regions will increase with decreasing genomic distance, the contacts between the upstream and downstream deletion-flanking regions in 22q11DS patient cells would be markedly enhanced. We indeed found such stronger contacts between the deletion-flanking regions in 22q11.2DS cell lines (**Fig. 1a; Supplementary Fig. 3a**). These regions of increased contact extended out to two million base pairs both upstream and downstream of the 22q11.2 deletion boundaries.

Following this observation we wanted to examine whether there is an effect on the chromatin marks concurrent to these increased chromosomal contact patterns. To do so we performed enrichment analysis in our ChIP-Seq data for significantly differential signal patterns for H3K27ac, H3K27me3 and CTCF, respectively. We found that both the upstream and downstream flanking regions of the 22q11.2 deletion were enriched with significantly differentially bound sites of both H3K27ac and H3K27me3 (**Fig. 2a,b**). For CTCF the downstream deletion-flanking region was enriched with significantly differentially bound sites (Fisher's exact test p = 2.53E-06) (**Fig. 2c**).

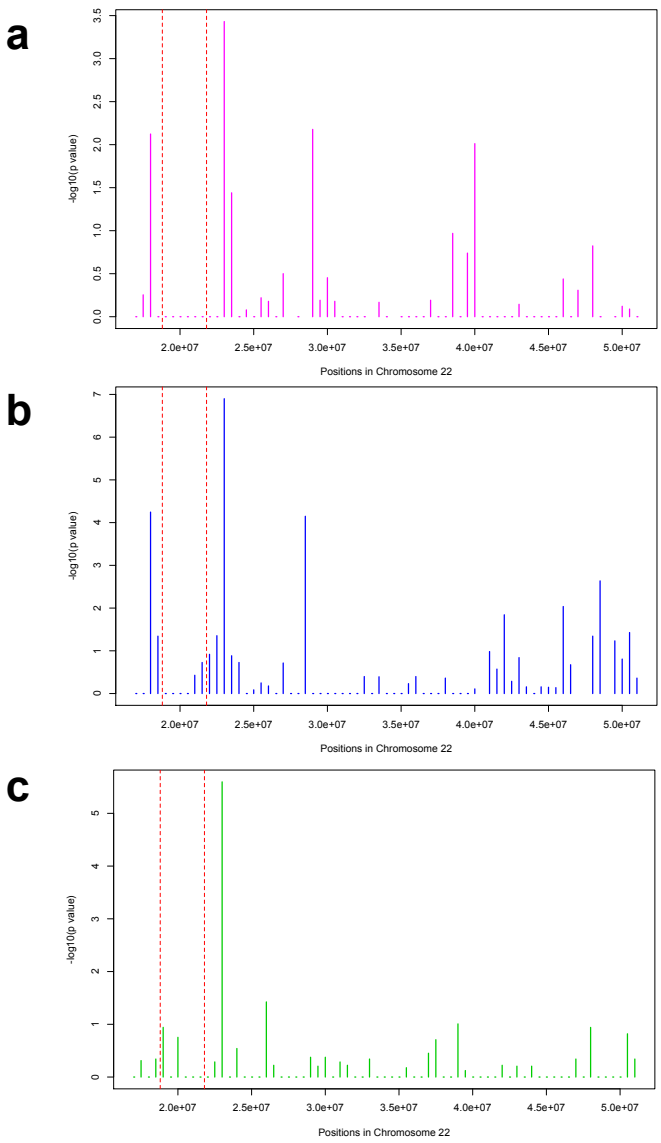

Figure 2. Distribution of significantly differentially enriched H3K27ac histone marks (a), H3K27me3 histone marks (b) and CTCF binding sites (c) along chromosome 22q. *Each point represents a 500 kbp bin. Red dashed lines mark the boundaries of the 3 Mbp deletion in 22q11.2.*

More specifically, within the upstream deletion-flanking region, from 18 to 18.5 Mbp, we found that 5 out of 24 sites with binding by H3K27ac and 6 out of 15 sites with binding

by H3K27me3 showed significantly differential binding (Fisher's exact test p = 0.0075 for H3K27ac and p = 5.67E-05 for H3K27me3 respectively). Intriguingly, for H3K27ac all of the 5 sites with significant differential binding were bound less strongly while for the same region for H3K27me3 all of the 6 sites with significant differential binding were bound more strongly in the 22q11DS patient lines. For the downstream region, from 23Mb to 23.5Mb, 5 out of 13 sites with H3K27ac binding and 11 out of 30 sites with H3K27me3 binding showed significantly differential binding (Fisher's exact test p = 0.0004 for H3K27ac and p = 1.26E-07 for H3K27me3 respectively). Again we observed the reciprocity between significantly differential changes for the two different histone marks: 4 out of 5 sites for H3K27ac gave a less strong signal while all of the 11 of such sites for H3K27me3 showed a stronger signal in the 22q11.2DS patient cell lines.

Such reciprocity in signal strengths between these two histone marks is a general feature of their principle of action and makes it much more likely that the observed changes are of physiological relevance.

Next we investigated whether there are gene expression changes in these same deletion-flanking regions. Based on the observed changes in histone marks we reasoned that gene expression in these regions could be downregulated in the 22q11DS patient lines, as H3K27ac is associated with active genes and H3K27me3 with repressed genes. We found that among the 4 genes with detectable expression in the deletion-upstream region from 18Mbp to 18.5 Mbp, the gene *BID* showed significantly decreased expression in 22q11.2DS patient lines while the other three remained unchanged. In the deletion-downstream region, from 23 Mbp to 23.5 Mbp, only one gene, *IGLL5,* had detectable levels of expression and we found it to exhibit significantly decreased expression in 22q11.2DS patient lines as well.

Taken together this part of our study shows that the effect of the 22q11.2 deletion is not limited to the genes within the deletion boundaries but also exerts extensive influence on its flanking regions on the level of intrachromosomal contacts, histone modifications and gene expression.

A/B compartments of the chromatin and the topological domain structure of the nuclear genome are affected by the 22q11.2 deletion

Previous studies of cell lines without large CNVs, have revealed that there is one level of organization where the chromatin is partitioned into two compartments, A and B, which correspond to active and inactive regions, respectively [20], and which can be derived from Hi-C data. We sought to determine whether the 22q11.2 deletion might lead to changes in these A/B compartments. Indeed when computing A/B compartments from our Hi-C data we observed that the eigenvectors changed signs in the 22q11.2 del region while all the other regions remained the same between 22q11.2DS patient and control cell lines (**Fig. 3a**). The original compartment that is spanning the deletion region in control cells is being partitioned into two shorter compartments with different eigenvectors signs, signifying a change in the A/B compartment structure in the deletion region.

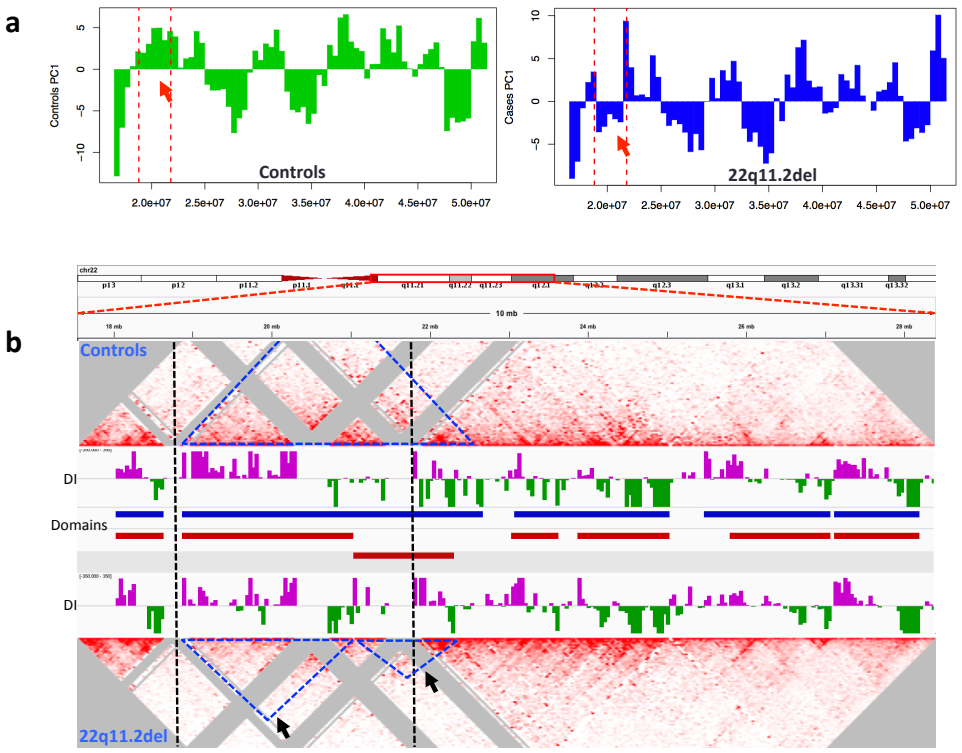

Figure 3. Change in A/B compartments and topological domain signal on chromosome 22q11. *(a) The A/B compartment spanning the 22q11 deletion in controls is partitioned into two compartments in the patient cell lines (red arrows). Red dashed lines: boundaries of 22q11.2del region. Shown is the first eigenvector for the principal component analysis of the normalized contact matrix. X-axis: position on chromosome 22q. Y-axis: value of the first eigenvector. (b) Normalized Hi-C contacts for 22q11.2del and control cell lines, displayed as a triangular heat-map that is overlayed on directionality indices (DI) and chromatin domains. The signal for the topological domain spanning the 22q11.2 deletion and its downstream region (blue triangle in controls) was broken into two shorter signals (blue triangles and black arrows in 22q11.2del). Black dashed lines: boundaries of 22q11.2del region. Regions with low mappability of reads were removed from the analysis and are shown in grey.*

Topological domains are a megabase-sized structural feature of the genome organization that is constituted of highly self-interacting chromosome regions [33]. Using our Hi-C and ChIP-Seq data we identified clear changes of the topological domain structure in the deletion-downstream flanking region of 22q11.2DS cell lines while the deletion-upstream topological domain structure was preserved (**Fig. 3b**). The topological domain spanning the 22q11.2 deletion and its downstream region was broken into two shorter domains across the downstream boundary of the deletion. Of note, this effect of the 22q11.2 deletion on the topological domain structure extended to 2 million base pairs downstream of the deletion region, where we observed another topological domain breaking into two shorter ones. Our results demonstrate that the 22q11.2 deletion can result in changing the order of topological domains both in the deletion region proper and its downstream regions.

Change of chromosomal *cis*-contacts involving the downstream flanking region of 22q11.2del

Based on the above findings that the genomic region downstream of the 22q11.2 deletion was affected on different levels of molecular regulation in 22q11.2DS patient cell lines, we next sought to investigate whether the presence of the 22q11.2 deletion also affected the chromosomal *cis*-contacts of the downstream deletion-flanking region with any other region on chromosome 22q. To do so, we analyzed our Hi-C data by calculating the fold change of contacts between the 21.5-22 Mbp window, which is situated right downstream of the 22q11.2 deletion, and all the other 1 Mbp-sized regions on chromosome 22q. As expected, we observed that region 17-18 Mbp, i.e. the breakpoint-proximal region right *upstream* of the deletion, showed the largest fold change (2.04) of contact with region 21.5-22 Mbp between 22q11DS and control cell lines, given that these regions were brought into

close proximity to each other by the 22q11.2 deletion (**Fig. 1a**).

The second largest fold change (1.96) of *cis*-contacts involving region 21.5-22 Mbp was for contacts with region 50-51 Mbp, i.e. towards the very telomeric end of chromosome 22q (**Fig. 1a**). Intriguingly, we also observed strong positive correlation between region 22-22.5 Mbp and region 50-50.5 Mbp for CTCF binding (Pearson's r = 0.933, p = 0.02) (**Supplementary Fig. 5a**) and between region 22-22.5 Mbp and region 50.5-51 Mbp for H3K27ac enrichment (Pearson's r = 0.811, p < 0.05) (**Supplementary Fig. 5b**). Furthermore there was weak correlation between region 22-22.5 Mbp and 50.5-51 Mbp for H3K27me3 enrichment (Pearson's r = 0.74, p = 0.090) (**Supplementary Fig. 5c**). Given that both region 21.5-22 Mbp and region 22-22.5 Mbp are in the downstream flanking region of the 22q11.2 deletion, our results strongly imply that increased chromosomal contacts between the downstream deletion-flanking region and the telomeric region 50-51 Mbp may be associated with the differential changes of histone modifications and CTCF binding that we found to be in correlation between these two regions.

To validate the increased chromosomal contact between the downstream deletion-proximal region and the telomeric end of 22q we performed DNA FISH on 5 cell lines with the 22q11.2 deletion and on 6 control cell lines, using FISH probes to loci in region 21.8-22.5 Mbp (RP11-47L18: chr22: 21,931,796 – 22,118,344) and in region 50-51Mbp (RP11-125K3: chr22: 50,149,996- 50287311). FISH showed that the downstream flanking region of the 22q11.2 deletion is significantly closer to region 50-51 Mbp in nuclear space in 22q11DS cell lines than in control cell lines (p value 0.008) (**Fig. 4; Supplementary Fig. 6**). Taken together, our results strongly indicate that the 22q11.2 deletion causes conformational changes on several levels on chromosome 22q.

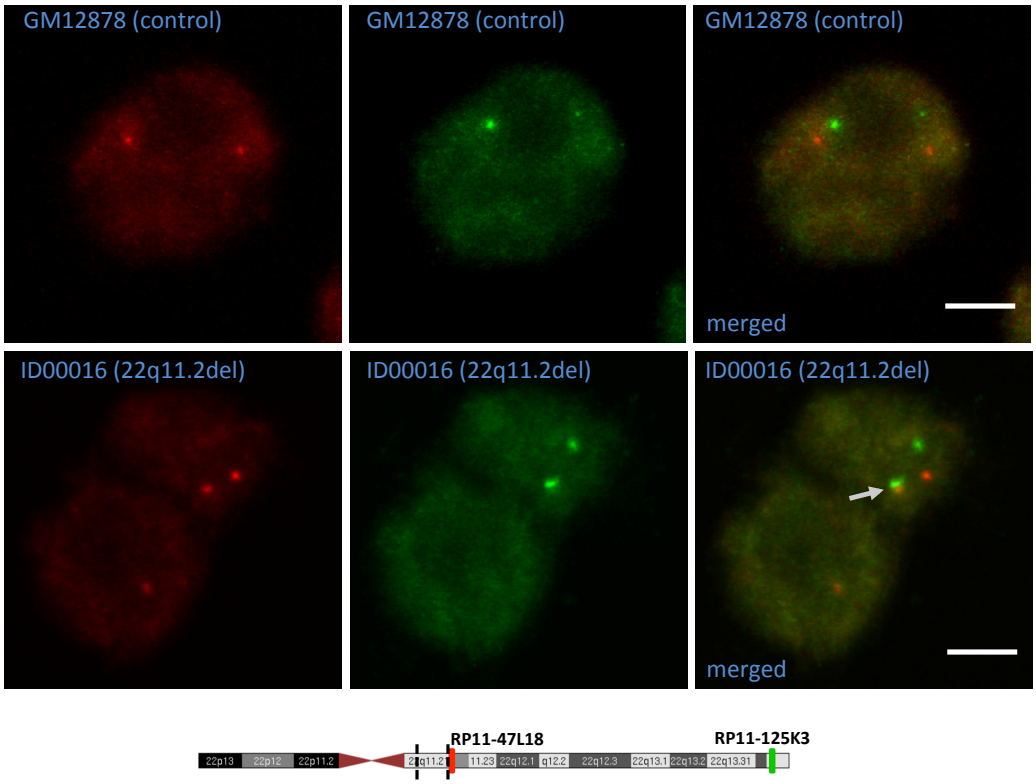

321

322 ***Figure 4. Examples of 3D FISH visualization of intra-chromosomal interaction changes.***
323 *The Hi-C predicted interaction regions of 21.8-22.5 Mbp and 50-51 Mbp on chromosome 22q*
324 *were visualized by 3D DNA FISH using BAC probes RP11-47L18 and RP11-125K3, labeled with*
325 *biotin (red) or digoxigenin (green). Arrow: an example for the red and green FISH probes in*
326 *close proximity in a cell carrying the 22q11.2 deletion. Scale bars are 5 µm. Red and green bars*
327 *on chromosome 22q indicate the locations of the biotin and digoxigenin FISH probes,*
328 *respectively. Black dashed lines indicate the position of the 3 Mbp deletion.*

329 **Global changes of interchromosomal contact patterns**

330 To explore the effect of the 22q11.2 deletion on *trans*-contacts, i.e. between any non-
331 homologous autosomes in the nucleus of 22q11.2DS patient lines, we analyzed our Hi-C
332 data for significantly different *trans*-contacts between 22q11DS and control cell lines. On

the genome-wide level, we found 272 *trans*-contacts with a p-value of less than 0.0001 (**Fig. 5a**). Interestingly the majority of these chromosomal *trans*-contacts did not involve chromosome 22q as one of the interacting partners. Notably, 56 of these interchromosomal contact signals are among the top 5% of the strongest *trans*-contacts (**Fig. 5b**). This enrichment of significantly different genome-wide chromosomal *trans*-contacts within the strongest *trans*-contacts is again highly statistically significant (Fisher's exact test $p < 2.2e-16$). We found many fewer significantly different genome-wide chromosomal *trans*-contacts by randomly swapping the assignment of 22q11.2 deletion and control status across our Hi-C data sets, by comparing within control cell lines and by comparing within 22q11.2del cell lines (**Supplementary Table 3**). None of these swapping analyses achieved the same enrichment. This indicates that a relevant amount of the significantly different genome-wide chromosomal *trans*-contacts is not due to random chromosomal motion or to as-of-yet unknown factors such as cell-culture variations across the lymphoblastoid cell lines. Rather, our analysis points to a genome-wide disturbance of the network of chromosomal *trans*-contacts that is at least in part attributable to the presence of the 22q11.2 deletion on chromosome 22q.

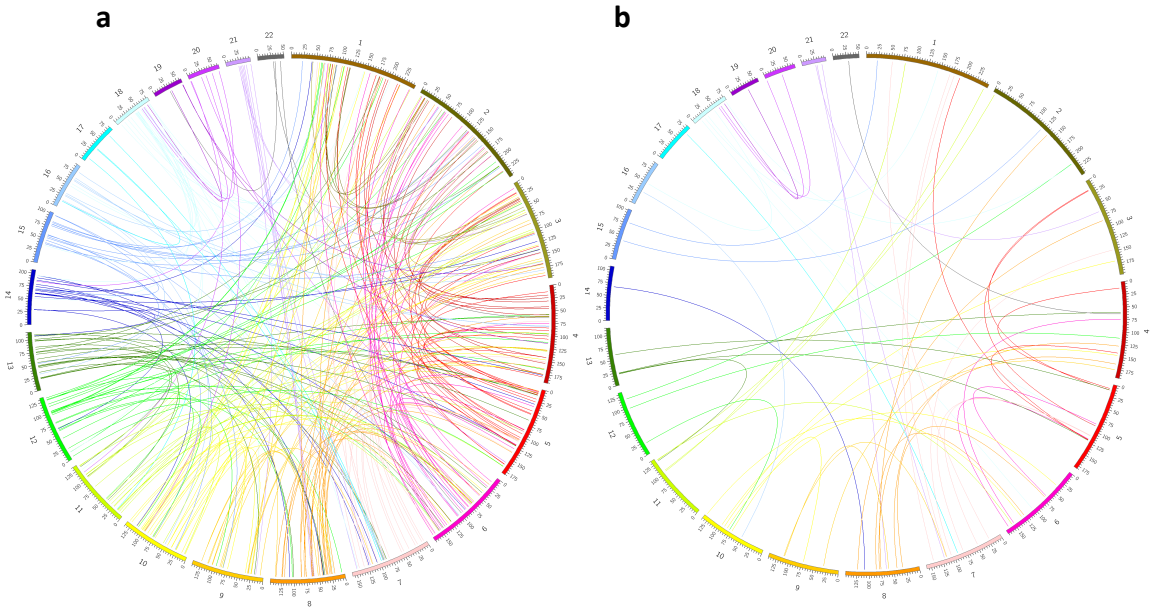

Figure 5. Genome-wide inter-chromosomal contact changes (either more or less frequent) determined by Hi-C analysis in 22q11.2del versus control cell lines. *(a) Circos plot of the inter-chromosomal contacts exhibiting differential interaction in 22q11.2del versus control cell lines at significance level of 0.0001. (b) Circos plot of the inter-chromosomal contacts exhibiting differential interaction in 22q11.2del versus control cell lines at significance level of 0.0001 and showing only the top 5% strongest inter-chromosomal contacts.*

Global changes of gene expression patterns

To investigate the global effect of the 22q11.2 deletion on gene expression, we performed differential expression analysis between the 22q11.2DS and control cell lines. Of the 11,374 genes with detectable levels of expression (FPKM > 0.5), 1,610 genes showed significantly

differential expression (FDR < 0.05). Gene ontology analysis indicated that these differentially expressed genes are enriched for genes involved in mitochondrial pathways such as the respiratory chain (n = 32, p value = 2.96E-11). KEGG pathway analysis demonstrated enrichment of genes involved in oxidative phosphorylation neurodegenerative diseases such as Parkinson's disease (**Fig. 6a**). Earlier studies have noted that there are several genes related to mitochondrial function that are located within the 22q11 deletion boundaries [34], therefore the pathways associated with this cellular function would have a high likelihood to be affected by the change in copy number. The enrichment for pathways related to neurodegenerative disorder is encouraging, as an association between 22q11DS and Parkinson's Disorder has been reported previously [35-37]. This reinforces the notion that the LCL cell culture model can be of relatively more relevance for the molecular study of 22q11DS in general.

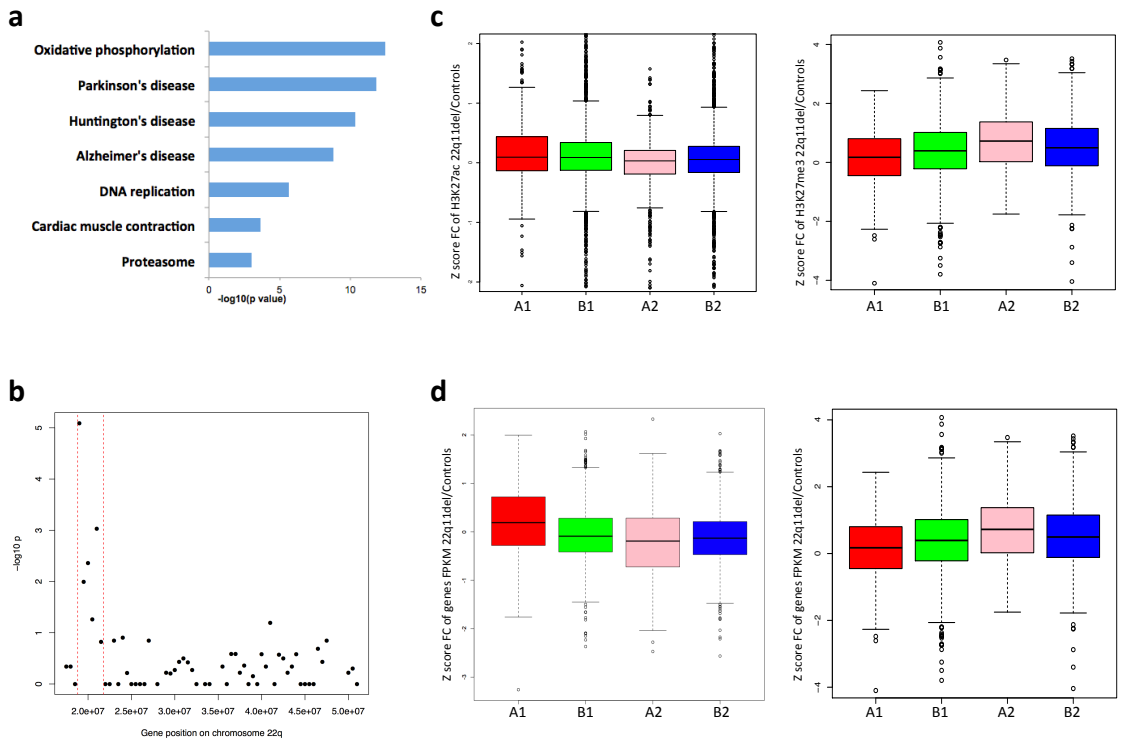

Figure 6. Differential expression analysis and correlation between gene expression and epigenetic profiles. *(a) KEGG pathway analysis for genes differentially expressed between 22q11.2del and control cell lines. (b) Enrichment analysis for chromosome 22q for differentially expressed genes. Red dashed lines mark the boundaries of 22q11.2del region. (c) Differentially expressed genes correlated with different H3K27ac and H3K27me3 signal strengths in 22q11.2del versus control cell lines. A1 represents genes significantly up-regulated in 22q11.2del cell lines while B1 represents non-significantly up-regulated genes; A2 represents genes significantly down-regulated in 22q11.2del cell lines while B2 represents non-significantly down-regulated genes. The y-axis shows the z-score transformed fold change of H3K27ac signals (left) or H3K27me3 signals (right) between 22q11.2del and control cell lines. (d) Differential H3K27ac and H3K27me3 signal strengths exhibited correlation with differential gene expression between 22q11.2del and control cell lines. A1 represents genes whose TSSs were significantly more marked by H3K27ac (left) or by H3K27me3 (right) in 22q11.2del cell lines. B1 represents genes with TSSs non-significantly more marked by H3K27ac (left) or by H3K27me3 (right). A2 represents genes whose TSSs were significantly less marked by H3K27ac (left) or by H3K27me3 (right) in 22q11.2del cell lines. B2 represents genes with TSSs non-significantly less marked by H3K27ac (left) or by H3K27me3 (right). The y-axis shows the z-score transformed fold change of genes' FPKM in 22q11.2del versus control cell lines.*

We next sought to identify whether genome-wide there were entire genomic regions that are enriched for differentially expressed genes. As expected, the most significant signals for this analysis were located in the 22q11.2 region (**Fig. 6b; Supplementary Fig. 7**). No other regions genome-wide achieved FDR corrected significance (**Supplementary Fig. 7**).

Correlation between histone modification and gene expression

To examine whether the gene expression changes are consistent with the histone modification changes, we assigned the H3K27ac and H3K27me3 peaks to their nearest genes based on the distance to their transcription start sites and for each gene, we only retained the closest peak for both histone marks. We observed that significantly upregulated genes in 22q11.2DS cell lines exhibited significantly higher fold change of H3K27ac enrichment (permutation test $p = 0.0140$) and significantly lower fold change of H3K27me3 enrichment (permutation test $p = 0.0018$) than genes non-significantly upregulated in 22q11.2DS cell lines (**Fig. 6c**). Consistently, significantly downregulated genes in 22q11.2DS cell lines exhibited significantly lower fold change of H3K27ac enrichment (permutation test $p = 0.0002$) but significantly higher fold change of H3K27me3 enrichment (permutation test $p = 0.0227$) than genes non-significantly down regulated in 22q11.2DS cell lines (**Fig. 6c**).

Moreover, genes whose transcription start sites (TSSs) showed significantly upregulated binding by H3K27ac in 22q11DS cell lines exhibited significantly higher fold change of expression (permutation test $p < 2.2e\text{-}16$) than those with non-significantly upregulated binding, while those TSSs showing significantly downregulated binding exhibited a significantly lower fold change of expression (permutation test $p = 0.0202$) than those with non-significantly downregulated binding (**Fig. 6d**). Consistently, genes whose TSSs showed significantly upregulated binding by H3K27me3 in 22q11DS showed significantly lower fold change of expression (permutation test $p = 0.0037$) while those with significantly downregulated binding exhibited significantly higher fold change of expression (permutation test $p = 0.0027$) between 22q11DS and control cell lines (**Fig. 6d**).

We also calculated the correlation between gene expression and H3K27ac binding

affinity across the individuals for all the genes with TSSs bound by H3K27ac. In line with the above results, we found significantly higher Pearson's correlation coefficients than the coefficients obtained from permutations (Wilcoxon rank sum test $p < 2.2e-16$) (**Supplementary Fig. 8a**). This difference was even more significant when we included the differential expressed genes (absolute fold change > 2) only (Wilcoxon rank sum test $p < 2.2e-16$) or the differential H3K27ac bound genes only into our analysis (Wilcoxon rank sum test $p < 2.2e-16$) (**Supplementary Fig. 8a**). Unsurprisingly, we also observed significantly higher Pearson's correlation coefficients between gene expression and H3K27me3 binding than the coefficients obtained from permutations for the differential expressed genes (absolute fold change > 2) only (Wilcoxon rank sum test $p = 9.72e-04$) and the differential H3K27me3 bound genes only (Wilcoxon rank sum test $p = 3.71e-06$) (**Supplementary Fig. 8b**). Together, our results demonstrated that gene expression changes are associated with histone modification changes in 22q11DS cell lines compared with control cell lines.

Effects of a large CNV on chromosome 1q21.1 on chromosome folding

To explore whether large CNVs other than the one on chromosome 22q11.2 can lead to changes in the patterns of chromosome folding, we performed Hi-C on two lymphoblastoid cell lines with a heterozygous deletion of approximately 1.35 Mbp in size on chromosome 1q21.1 (1q21.1del). This deletion is strongly associated with the development of schizophrenia [38-40]. As for the 22q11.2 deletion, we observed that both *cis*-contacts and *trans*-contacts between the 1q21.1 deletion regions and other regions were decreased in 1q21.1del cell lines relative to control cell lines (**Fig. 7a,b**). As observed in the 22q11DS cell lines, in the 1q21.2del cell lines there was an increase of intrachromosomal contacts between the regions directly flanking the main CNV of 1q21.1 (**Fig. 7a**). Analysis of A/B

compartments showed that the eigenvector sign of the downstream boundary region of the 1q21.1 deletion was inverted (**Fig. 7c**), showing that also on the level of chromatin compartmentalization the large CNV on 1q21.2 can have effects, similar to the large CNV on 22q11.2. Taken together the large deletion CNV on chromosome 1q21.1 exhibited similar effects on chromosomal *cis*-contacts and *trans*-contacts as the large deletion CNV on chromosome 22q11.2, which points towards our findings in 22q11DS being generalizable across large neuropsychiatric CNVs.

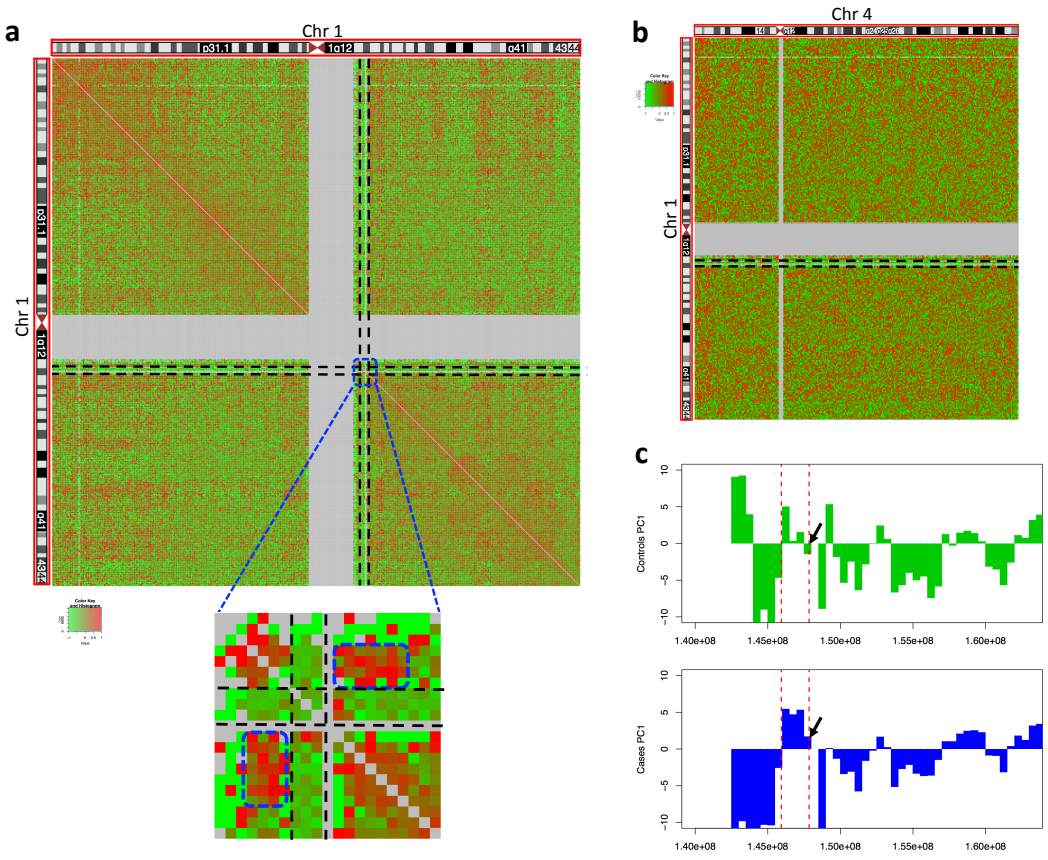

Figure 7. Effect of the large deletion CNV on 1q21.1 on chromosome conformation. *(a) Fold change of cis-contacts of chromosome 1 in 1q21.1del versus control cell lines. Blue boxes mark the regions of increased contacts between the upstream and downstream flanking regions of the 1q21.1 deletion. (b) Fold change of trans-contacts between chromosome 1 and 4*

in 1q21.1del cell lines versus control cell lines. Black dashed lines mark the boundaries of the 1q21.1 deletion. Each cell in the heatmap represents the inter-chromosomal contact level between two 500 kbp regions. (c) Change in A/B compartments on chromosome 1q21. Upper panel: control cell lines. Lower panel: 1q21.1del cell lines. Shown is the first eigenvector for the principal component analysis on the normalized contact matrix of chromosome 1, for 1q21.1del and control cell lines. X-axis: position on chromosome 1q. Y-axis: value of the first eigenvector. Black arrows indicate the location of change in the eigenvector sign in the downstream boundary region of 1q21.1, in 1q21.1del cell lines.

Discussion

Large CNVs are an important feature of the genetic architecture of several major neurodevelopmental psychiatric disorders as well as of conditions involving aberrant morphology of many organ systems. Their effects on the level of phenotype are complex and the molecular mechanisms mediating these effects are very incompletely understood. While it is still a good assumption that a considerable portion of these mechanisms are a direct consequence of the copy number change of the genes within a given CNV's boundaries and the resulting changes in expression levels for these genes, it also seems plausible to investigate whether additional levels of complexity exist regarding the effects of a large CNV across multiple layers of the control of gene activity. This plausibility stems from several observations and lines of reasoning. Namely there are large numbers of genes affected genome wide and far distal from the main CNV, and expression changes within CNV boundaries do not always follow exactly the change in copy number. This leads us to consider the basic principles that govern organizational features of the nucleus and the chromatin such as regulatory domains being bounded by protein factors that recognize binding sites in the DNA sequence which in turn could be affected (i.e. deleted or

duplicated) by a CNV, or long-range chromosome contacts being also influenced by the length of the involved chromosomes (and that length being changed by large CNVs). Finally there have been several recent reports about mutations in chromatin remodeling genes in the context of neuropsychiatric disorders pointing to the importance of proper molecular management on the epigenomic level in these conditions.

Here we studied the effects of the important large CNV on chromosome 22q11.2, and in a more limited fashion the effects of the large CNV on chromosome 1q21.2, on chromatin conformation including long-range chromosome contacts and domain formation, epigenetic profiles and gene expression. To our knowledge, this is the first study of changes in chromatin conformation and epigenetic profile changes caused by deletions on 22q11.2, and 1q21.2, or any such large CNVs with strong relevance to organ development and in particular brain development and neuropsychiatric disorders. We observed dosage effects of the large CNVs on long-range chromosome contacts, chromatin domains and epigenetic profiles as well as on gene expression. More specifically we found increased contacts between upstream and downstream flanking regions of the 22q11.2 deletion in 22q11DS cell lines in contrast with control cell lines. Interestingly, both upstream and downstream regions of the 22q11.2 deletion were enriched with differentially binding sites of H3K27ac and H3K27me3 while downstream regions were also enriched with differentially binding sites of CTCF. Importantly, the gene expression changes in these regions were consistent with the histone modification changes as less H3K27ac binding and more H3K27me3 binding reflect decreased gene expression in 22q11Ds cell lines. Based on the above findings, it is tempting to speculate that increased contacts between upstream and downstream flanking regions of the 22q11.2 deletion contribute to gene expression changes via the coordinated changes of epigenetic profiles in these flanking regions.

506 Although we found chromosome contacts to be correlated with both the epigenetic
507 profiles and the gene expression changes in the flanking regions of the 22q11.2 deletion, we
508 did not observe significant correlation either between chromosome contact changes and
509 gene expression changes or between chromosome contact changes and epigenetic profile
510 changes (data not shown) on the genome-wide level. Moreover, we did not observe the end
511 of chromosome 22 (50-51Mb) to be enriched with differentially expressed genes (2 out of
512 24 genes) despite the Hi-C finding, validated by FISH, of significantly increased contacts
513 with the downstream flanking region of the 22q11.2 deletion in 22q11.2DS cell lines. Our
514 results indicate that chromosome conformation changes caused by the 22q11.2 deletion
515 contribute to gene expression changes and epigenetic profile changes between 22q11.2DS
516 and control cell lines but not always in a clearly and linearly deterministic way.

517 However, we did observe significant positive correlation between H3K27ac changes
518 and gene expression changes but negative correlation between H3K27me3 and gene
519 expression changes on the genomic level. These findings demonstrated that the epigenetic
520 profiles were reshaped genome-wide to cause extensive gene expression changes in
521 22q11.2DS cell lines.

522 The dosage effects of the deletion on *cis*- and *trans*-contacts and the increased
523 chromosomal contacts between upstream and downstream deletion-flanking regions in
524 22q11Ds cell lines were also observed in cell lines with the 1q21.1 deletion. The similar
525 results that were obtained on that level of observation for the 22q11.2 deletion and the
526 1q21.1 deletion would suggest that these changes caused by a large deletion CNV are
527 universal for such chromosomal aberrations instead of specific to the 22q11.2 deletion.

528 As a cautionary note on the technical level, we demonstrated here that for genomes
529 with a large deletion CNV the appropriate normalization methods for Hi-C data have to be

chosen with great care to avoid false findings. For instance we would have reached the conclusion that the chromosomal contacts within the deletion regions are not decreased in cell lines with deletion compared with control cell lines if the hiclib software package [22] had been used for normalization of Hi-C data, instead of the hicpipe package [21].

Lastly, we also observed A/B chromatin compartment changes and changes in the signal from topological domain analyses across the 22q11.2 deletion region. This is the first time that such a phenomenon has been reported in this context. Earlier, Lupiáñez et al. [41], using the 4C assay, demonstrated in a mouse model as well as in human lines from patients with rare malformations of the limbs, that large structural changes in the genomic sequence can affect the topological domain architecture directly on top of the sequence change, giving further support to our Hi-C based findings in 22q11.2 and 1q21.1 deletion lines. It is important to remember that, just as for earlier studies that were reporting on A/B compartments and topological domains (in non-CNV genomes), our analysis resulted from combining the sequencing data of two homologous chromosomes. Only once haplotype phasing of the genomes in question will be available will one be able to determine whether the chromosome 22q with large deletion or the one without large deletion, or some combination of the two, is driving such changes in the domain signals (the deletion-carrying domain being the main cause for the change in signal certainly being the initial hypothesis). Whether the observed chromosomal contact changes on chromosome 22q are existent only on one chromosome 22q (again probably the one carrying the large CNV) or emanate from both of the two homologous chromosomes is currently unknown and will be worth investigating when haplotype-phasing data is available.

In summary, we found dosage effects of the large deletion CNV on chromosome 22q11.2 on long-range chromosome contacts, chromatin organization, epigenetic profiles

554 and gene expression. Extensive changes on these levels caused by the 22q11.2 deletion are
555 global and seem to be rippling along the entire chromosome carrying the deletion as well as
556 across the entire nucleus rather than being confined to the deletion region only. Such effects
557 had never been shown before outside of cancer cell lines [42]. Furthermore, in contrast to the
558 findings in cancer cells we used a larger cohort of individual patient cell lines, with all lines
559 carrying only one main large CNV that is clearly and strongly associated in a causative
560 manner with a neurodevelopmental phenotype. This, in contrast to the two cancer cell lines
561 that each carried multiple large CNVs which could also have been a consequence rather
562 than a cause of the disease phenotype, makes it much more likely that the higher-order
563 effects of the large CNVs that we observed may be contributing to the molecular etiology of
564 the disorders in question. This point is further strengthened by another recent paper [43],
565 where the authors describe studying the effects of large CNVs on chromosome 16p11 on
566 chromosome interactions. These large CNVs are almost as strongly associated with
567 neurodevelopmental disorders than the large CNV on 22q11.2. While the study on the
568 16p11 CNVs used a somewhat smaller number of cell lines than our study and also used 4C
569 as a method of discovery, which is, unlike the Hi-C method used by us, not able to detect
570 changes in a global and unbiased fashion, it is one more independent piece of supporting
571 evidence for the biological validity and general relevance of the findings which we describe
572 here.

573 While we were able to show possible correlations across several pairs of the molecular
574 levels that we assayed in this study there are other combinations of molecular levels that
575 show no obvious connection in our data. We believe that this could be a function of either
576 the developmental time point or the cell type, or both, being removed from those where the
577 22q11.2 and 1q21.1 deletions most likely exert some of their strongest effects (e.g. during
578 embryonal development and in cells of the developing central nervous system). The clear

579 effects that we were able to observe in lymphoblastoid cell lines could represent the
580 afterglow of a molecular tragedy that played out earlier in the development of various
581 organs in the patients carrying these deletions. At the same time the strength of this
582 afterglow would hint at the strength of the effects that impacted across various levels of
583 molecular control and gene regulation by CNVs of this size.

584 **Methods**

585 **Cell lines and data generation for this study.** All cell lines were either acquired from the
586 Coriell cell repository (cell lines IDs starting with GM or ID) or were taken from the
587 Molecular Genetics of Schizophrenia (MGS) cohort (dbGaP Study Accession:
588 phs000167.v1.p, cell lines 52425 and 82699), and were appropriately consented. The Hi-C
589 assay was carried out according to the original protocol [20], with several modifications. ChIP-
590 Seq was performed as described in previous studies [44,45]. The RNA-seq libraries were
591 generated according as in [46]. All experimental procedures are described in the
592 **Supplementary Information**.

593 **Hi-C Data analysis.** All Hi-C data were produced using Illumina paired-end sequencing with
594 a read length 2 x 101 bp. As there might be ligation junctions in the reads, we performed
595 iterative mapping using bowtie2 as in Imakaev et al. 2012 [22]. Briefly, we computationally cut
596 all the reads to 25 bp first and mapped them to human genome (hg19). Then we extended
597 the non-uniquely mapped reads by 5 bp to 30 bp and mapped them again. This process was
598 repeated until the read length was extended to 101 bp. This iterative mapping did improve
599 the mapping rate (**Supplementary Table 4**). Each read end was mapped separately using
600 the single ends mode. Only uniquely mapping reads were used and PCR duplicate read pairs
601 were removed. We only included autosomes in our study. The filtered contact number is
602 listed in **Supplementary Table 5**.

603 We compared three different data normalization methods: hiclib [22], hicpipe [21] and
604 HiCNorm [23]. All of the three tools were run using the default parameters except for the
605 segment length threshold being set to 600 bp. We chose normalized metrics on hicpipe for
606 the following analyses, using a bin size of 40 kb for topological domain analysis and of 500
607 kb for the other analyses. The total number of contacts was normalized for each sample
608 before combining cell lines in each category (control, 22q11del and 1q21del, respectively).
609 Fold changes of log2 transformed mean contacts between deletion cell lines and control cell
610 lines were calculated by (deletion – control)/control.

611 To identify the differential interchromosomal contacts, we only included contacts with
612 at least 1 supporting read pair in each of the cell lines. Differential contacts analysis was
613 conducted by Student's t-test using the normalized metrics. Fisher's exact test was used to
614 assess the enrichment of differential contacts within the top 5% strongest contacts. We also
615 performed the same analysis by permuting the control and 22q11del status of the cell lines
616 ten times. Comparison within control cell lines and within 22q11del cell lines were
617 performed by randomly dividing the cell lines into two groups three times.

618 Identification of A and B compartments was performed as in Lieberman et al. 2009 [20]
619 and topological domains were identified as in Dixon et al. 2012 [33]. We modified the
620 algorithm for identifying topological domains such that when calculating the direction index
621 for a given bin we will exclude neighboring bins that are spanned by segmental duplications
622 as well as the bins on the opposite side of the given bin and equidistant to the given bin than
623 the bins spanned by segmental duplications (even if such symmetrical bins are not spanned
624 by segmental duplications themselves). For topological domain analysis, we pooled the raw
625 data of all the samples for each category to obtain sufficient Hi-C sequencing coverage
626 before normalization.

3D FISH. Two human DNA BACs (clones RP11-47L18 and RP11-125K3) covering two distinct regions of chromosome 22 were labeled with biotin or digoxigenin (DIG) by nick translation kit (Roche Applied Sciences) to make FISH probes (Roche). In-situ hybridization was performed according to the method published by [47], with several modifications. Experimental details and data analysis could be found in the **Supplementary Information**.

Differential expression analysis. All RNA-seq data were generated using Illumina paired-end sequencing with read length 101 bp. Reads were mapped to hg19 and transcriptome reference with TopHat 2 [48]. TopHat 2 was run using default parameters but with the coverage search being turned off. The mapped reads were analyzed by Cufflinks [49]. Differential expression was estimated with Cuffdiff 2 [50]. We excluded the genes with low expression (FPKM < 0.5) from downstream analysis.

Pathway analysis of significantly differential expressed genes was conducted with DAVID [51] using all the expressed genes as background.

ChIP-Seq data analysis. All ChIP-Seq data were generated using Illumina paired-end sequencing with read length 101 bp. Reads were aligned to hg19 with BWA-MEM using default parameters [52]. Reads with low mapping quality (< 30) were removed. PCR duplicate reads were removed using Picard (http://broadinstitute.github.io/picard). As a quality control, we calculated the normalized strand cross-correlation coefficient (NSC) and relative strand correlation (RSC) [53] to assess the signal-to-noise ratios. All the data showed higher NSC than RSC (**Supplementary Fig. 9**). Replicates for the same cell line on average showed higher correlation than datasets from different cell lines (**Supplementary Fig. 10**).

For CTCF and H3K27ac, we used MACS2 [54] to call narrow peaks with default parameters. For H3K27me3, we used the broad peak calling in MACS2. For all peak calling,

650 we used the corresponding whole-cell extract input library as background. For differential
651 bound analysis, we used the R package DiffBind [55] with the effective library size for read
652 counts normalization. Then DBA_DESEQ2 method was employed to conduct the differential
653 bound analysis. Signal artifact blacklist regions were excluded from our analysis
654 (http://hgdownload.cse.ucsc.edu/goldenPath/hg19/encodeDCC/wgEncodeMapabil
655 ity).

656 **Enrichment analysis.** For the enrichment analysis of differentially expressed genes we
657 divided each chromosome into 500 kbp bins. Within each bin, we calculated the total
658 number of expressed genes and the number of genes with significantly differential
659 expression between 22q11del and control cell lines. Then we conducted Fisher's exact test
660 to identify bins enriched with significantly differentially expressed genes against the
661 background of the whole genome.

662 For the analysis of differentially enriched sites for CTCF, H3K27ac and H3K27me3, we
663 also used 500 kbp bins. Log2 transformed fold changes of normalized read numbers in
664 binding sites between 22q11del and control cell lines were further transformed to Z-scores.
665 We considered binding sites with Z-score >2 or < -2 as significantly bound sites. Then
666 within each 500 kbp bin, we calculated the total number of binding sites and the number of
667 significantly differentially enriched sites between 22q11del and control cell lines. Then we
668 conducted Fisher's exact test to identify bins with significantly differentially enriched sites
669 against the background of the whole genome.

670 **Correlation analysis of gene expression and histone modification.** To estimate the
671 correlation between gene expression and histone modification, we assigned each binding
672 site of H3K27ac and H3K27me3 to its nearest ENSEMBL TSS using the R package
673 ChIPpeakAnno [56]. If a TSS was associated with multiple binding sites, only the nearest

674 binding site was retained. We then used this assignment for downstream correlation
675 analysis. To determine the cutoff for the distance in which binding sites are associated with
676 TSSs, we plotted the distribution of distances between binding sites and their assigned TSSs
677 (**Supplementary Fig. 11**). Based on the distribution, we set the cutoff to distance to TSS to
678 ± 1 kbp for H3K27ac and to ± 5 kbp for H3K27me3.

679 To investigate the effects of histone modifications on gene expression, we divided the
680 genes into two categories based on the differential expression analysis: differentially
681 expressed genes (FDR < 0.05) (category A) and not differentially expressed genes (FDR >
682 0.05) (category B). Within each category, we further categorized the genes into two groups:
683 up-regulated expressed genes (A1, B1) and down-regulated expressed genes (A2, B2) in
684 22q11del cell lines relative to control cell lines. Then for the genes within each of the four
685 groups (A1, B1, A2, B2), we calculated the Z-score transformed fold changes of the
686 normalized read counts in the TSS binding sites of histone marks between 22q11del and
687 control cell lines. To obtain the statistical significance of the fold change differences
688 between A1 and B1 and between A2 and B2, we performed permutation tests with 9,999
689 permutations.

690 We also carried out the reverse analysis. TSS binding sites of histone marks were
691 partitioned into two categories based on the differential bound analysis: differentially
692 bound sites (|Z-score| > 1 for H3K27ac, |Z-score| > 2 for H3K27me3) (category A) and non-
693 differentially bound sites (|Z-score| < 1 for H3K27ac, |Z-score| < 2 for H3K27me3) (category
694 B). Within each category, we further categorized the binding sites into two groups: up-
695 regulated bound sites (A1, B1) and down-regulated bound sites (A2, B2) in 22q11del cell
696 lines. Then we calculated the fold changes of the genes' FPKM between 22q11del and
697 control cell lines within each group. Permutation tests were performed with 9,999

permutations to obtain statistical significance.

To estimate the correlation between gene expression and histone modification in a direct way, we calculated Pearson's correlation coefficient between gene's FPKM and normalized read counts in the corresponding TSS binding site for each gene across all of the cell lines. To obtain statistical significance, we first permuted genes' FPKM across the cell lines for each TSS 10 times to assess the background correlation levels, and then performed the Wilcoxon rank sum test between the observed correlation coefficients and the background correlation coefficients. We also performed the same analysis using the differentially expressed genes only and differentially enriched binding sites only.

Correlation analysis for epigenetic marks. To assess the correlation of epigenetic marks binding between different regions on the same chromosomes, we divided the chromosomes into 500 kbp bins. Within each bin, we calculated the mean value of the normalized read counts for all the binding sites of each epigenetic mark. Then we calculated the Pearson's correlation coefficients of obtained mean values across the cell lines between any two bins on the same chromosomes.

Data availability. Hi-C, ChIP-Seq and RNA-Seq data from this study have been submitted to the NCBI Gene Expression Omnibus (GEO; http://www.ncbi. nlm.nih.gov/geo/) under accession number GSE76922.

Competing interests

The authors declare that no competing interests exist.

Authors' contributions (in order of position in Authors List)

YZ contributed to study design and produced experimental data, XZ contributed to study design, carried out data analysis and contributed to writing the paper, XZ contributed to study design and carried out data analysis, CP produced experimental data and contributed to data interpretation, MSH produced experimental data, TW produced experimental data, JY produced experimental data, SMW and AEU conceived of and designed the study, directed data production and data analysis and wrote the paper.

Acknowledgments

This research was supported by external funding from the National Institute of Mental Health (NIMH) (grant number: MH100010), NARSAD and the March of Dimes, as well as funds from Stanford Pediatric Research Fund (Grant number: UL1 RR025744) and departmental funds from the Stanford Department of Psychiatry and Behavioral Sciences.

We thank Dr. Eitan Yaffe (Stanford University) for his advice on the use of hicpipe.

References

1 Kirov, G. CNVs in neuropsychiatric disorders. *Hum Mol Genet* **24**, R45-49, doi:10.1093/hmg/ddv253 (2015).

2 Torres, F., Barbosa, M. & Maciel, P. Recurrent copy number variations as risk factors for neurodevelopmental disorders: critical overview and analysis of clinical implications. *J Med Genet* **53**, 73-90, doi:10.1136/jmedgenet-2015-103366 (2016).

3 Auton, A. *et al.* A global reference for human genetic variation. *Nature* **526**, 68-74, doi:10.1038/nature15393 (2015).

4 Sudmant, P. H. *et al.* An integrated map of structural variation in 2,504 human genomes. *Nature* **526**, 75-81, doi:10.1038/nature15394 (2015).

5 Korbel, J. O. *et al.* Paired-end mapping reveals extensive structural variation in the human genome. *Science* **318**, 420-426, doi:10.1126/science.1149504 (2007).

6 Abecasis, G. R. *et al.* A map of human genome variation from population-scale sequencing. *Nature* **467**, 1061-1073, doi:10.1038/nature09534 (2010).

7 Mills, R. E. *et al.* Mapping copy number variation by population-scale genome sequencing. *Nature* **470**, 59-65, doi:10.1038/nature09708 (2011).

8 Santos, J. L. *et al.* Copy number polymorphism of the salivary amylase gene: implications in human nutrition research. *J Nutrigenet Nutrigenomics* **5**, 117-131, doi:10.1159/000339951 (2012).

9 Gavin, D. P. & Floreani, C. Epigenetics of schizophrenia: an open and shut case. *Int Rev Neurobiol* **115**, 155-201, doi:10.1016/B978-0-12-801311-3.00005-6 (2014).

10 Fullard, J. F. *et al.* Understanding the genetic liability to schizophrenia through the neuroepigenome. *Schizophr Res*, doi:10.1016/j.schres.2016.01.039 (2016).

11 Nestler, E. J., Peña, C. J., Kundakovic, M., Mitchell, A. & Akbarian, S. Epigenetic Basis of Mental Illness. *Neuroscientist*, doi:10.1177/1073858415608147 (2015).

12 Mitchell, A. C. *et al.* The genome in three dimensions: a new frontier in human brain research. *Biol Psychiatry* **75**, 961-969, doi:10.1016/j.biopsych.2013.07.015 (2014).

13 Barnard, R. A., Pomaville, M. B. & O'Roak, B. J. Mutations and Modeling of the Chromatin Remodeler CHD8 Define an Emerging Autism Etiology. *Front Neurosci* **9**, 477, doi:10.3389/fnins.2015.00477 (2015).

14 Vallianatos, C. N. & Iwase, S. Disrupted intricacy of histone H3K4 methylation in neurodevelopmental disorders. *Epigenomics* **7**, 503-519, doi:10.2217/epi.15.1 (2015).

15 Zhubi, A., Cook, E. H., Guidotti, A. & Grayson, D. R. Epigenetic mechanisms in autism spectrum disorder. *Int Rev Neurobiol* **115**, 203-244, doi:10.1016/B978-0-12-801311-3.00006-8 (2014).

16 Biswas, A. B. & Furniss, F. Cognitive phenotype and psychiatric disorder in 22q11.2 deletion syndrome: A review. *Res Dev Disabil* **53-54**, 242-257, doi:10.1016/j.ridd.2016.02.010 (2016).

17 Swillen, A. & McDonald-McGinn, D. Developmental trajectories in 22q11.2 deletion. *Am J Med Genet C Semin Med Genet* **169**, 172-181, doi:10.1002/ajmg.c.31435 (2015).

18 Schneider, M. *et al.* Psychiatric disorders from childhood to adulthood in 22q11.2 deletion syndrome: results from the International Consortium on Brain and Behavior in 22q11.2 Deletion Syndrome. *Am J Psychiatry* **171**, 627-639, doi:10.1176/appi.ajp.2013.13070864 (2014).

19 Urban, A. E. *et al.* High-resolution mapping of DNA copy alterations in human chromosome 22 using high-density tiling oligonucleotide arrays. *Proc Natl Acad Sci U S A* **103**, 4534-4539, doi:10.1073/pnas.0511340103 (2006).

20 Lieberman-Aiden, E. *et al.* Comprehensive mapping of long-range interactions reveals folding principles of the human genome. *Science* **326**, 289-293, doi:10.1126/science.1181369 (2009).

21 Yaffe, E. & Tanay, A. Probabilistic modeling of Hi-C contact maps eliminates systematic biases to characterize global chromosomal architecture. *Nat Genet* **43**, 1059-1065, doi:10.1038/ng.947 (2011).

22 Imakaev, M. *et al.* Iterative correction of Hi-C data reveals hallmarks of chromosome organization. *Nat Methods* **9**, 999-1003, doi:10.1038/nmeth.2148 (2012).

23 Hu, M. *et al.* HiCNorm: removing biases in Hi-C data via Poisson regression. *Bioinformatics* **28**, 3131-3133, doi:10.1093/bioinformatics/bts570 (2012).

24 Schmid, M. W., Grob, S. & Grossniklaus, U. HiCdat: a fast and easy-to-use Hi-C data analysis tool. *BMC Bioinformatics* **16**, 277, doi:10.1186/s12859-015-0678-x (2015).

25 Servant, N. *et al.* HiC-Pro: an optimized and flexible pipeline for Hi-C data processing. *Genome Biol* **16**, 259, doi:10.1186/s13059-015-0831-x (2015).

26 Heinz, S. *et al.* Simple combinations of lineage-determining transcription factors prime cis-regulatory elements required for macrophage and B cell identities. *Mol Cell* **38**, 576-589, doi:10.1016/j.molcel.2010.05.004 (2010).

27 Li, W., Gong, K., Li, Q., Alber, F. & Zhou, X. J. Hi-Corrector: a fast, scalable and memory-efficient package for normalizing large-scale Hi-C data. *Bioinformatics* **31**, 960-962, doi:10.1093/bioinformatics/btu747 (2015).

28 Servant, N. *et al.* HiTC: exploration of high-throughput 'C' experiments. *Bioinformatics* **28**, 2843-2844, doi:10.1093/bioinformatics/bts521 (2012).

29 Shavit, Y. & Lio', P. Combining a wavelet change point and the Bayes factor for analysing chromosomal interaction data. *Mol Biosyst* **10**, 1576-1585, doi:10.1039/c4mb00142g (2014).

30 Sauria, M. E., Phillips-Cremins, J. E., Corces, V. G. & Taylor, J. HiFive: a tool suite for easy and efficient HiC and 5C data analysis. *Genome Biol* **16**, 237, doi:10.1186/s13059-015-0806-y (2015).

31 Rao, S. S. *et al.* A 3D map of the human genome at kilobase resolution reveals principles of chromatin looping. *Cell* **159**, 1665-1680, doi:10.1016/j.cell.2014.11.021 (2014).

32 Rees, E. *et al.* Evidence that duplications of 22q11.2 protect against schizophrenia. *Mol Psychiatry* **19**, 37-40, doi:10.1038/mp.2013.156 (2014).

33 Dixon, J. R. *et al.* Topological domains in mammalian genomes identified by analysis of chromatin interactions. *Nature* **485**, 376-380, doi:10.1038/nature11082 (2012).

34 Maynard, T. M. *et al.* Mitochondrial localization and function of a subset of 22q11 deletion syndrome candidate genes. *Mol Cell Neurosci* **39**, 439-451, doi:10.1016/j.mcn.2008.07.027 (2008).

827 35 Butcher, N. J. *et al.* Association between early-onset Parkinson disease and
828 22q11.2 deletion syndrome: identification of a novel genetic form of
829 Parkinson disease and its clinical implications. *JAMA Neurol* **70**, 1359-1366,
830 doi:10.1001/jamaneurol.2013.3646 (2013).
831 36 Boot, E. *et al.* Movement disorders and other motor abnormalities in adults
832 with 22q11.2 deletion syndrome. *Am J Med Genet A* **167A**, 639-645,
833 doi:10.1002/ajmg.a.36928 (2015).
834 37 Mok, K. Y. *et al.* Deletions at 22q11.2 in idiopathic Parkinson's disease: a
835 combined analysis of genome-wide association data. *Lancet Neurol* **15**, 585-
836 596, doi:10.1016/S1474-4422(16)00071-5 (2016).
837 38 Stefansson, H. *et al.* Large recurrent microdeletions associated with
838 schizophrenia. *Nature* **455**, 232-236, doi:10.1038/nature07229 (2008).
839 39 Consortium, I. S. Rare chromosomal deletions and duplications increase risk
840 of schizophrenia. *Nature* **455**, 237-241, doi:10.1038/nature07239 (2008).
841 40 Levinson, D. F. *et al.* Copy number variants in schizophrenia: confirmation of
842 five previous findings and new evidence for 3q29 microdeletions and VIPR2
843 duplications. *Am J Psychiatry* **168**, 302-316,
844 doi:10.1176/appi.ajp.2010.10060876 (2011).
845 41 Lupiáñez, D. G. *et al.* Disruptions of topological chromatin domains cause
846 pathogenic rewiring of gene-enhancer interactions. *Cell* **161**, 1012-1025,
847 doi:10.1016/j.cell.2015.04.004 (2015).

42 Taberlay, P. C. *et al.* Three-dimensional disorganization of the cancer genome occurs coincident with long-range genetic and epigenetic alterations. *Genome Res* **26**, 719-731, doi:10.1101/gr.201517.115 (2016).

43 Loviglio, M. N. *et al.* Chromosomal contacts connect loci associated with autism, BMI and head circumference phenotypes. *Mol Psychiatry*, doi:10.1038/mp.2016.84 (2016).

44 Kasowski, M. *et al.* Extensive variation in chromatin states across humans. *Science* **342**, 750-752, doi:10.1126/science.1242510 (2013).

45 Raha, D., Hong, M. & Snyder, M. ChIP-Seq: a method for global identification of regulatory elements in the genome. *Curr Protoc Mol Biol* **Chapter 21**, Unit 21.19.21-14, doi:10.1002/0471142727.mb2119s91 (2010).

46 Abyzov, A. *et al.* Somatic copy number mosaicism in human skin revealed by induced pluripotent stem cells. *Nature* **492**, 438-442, doi:10.1038/nature11629 (2012).

47 Yao, J., Fetter, R. D., Hu, P., Betzig, E. & Tjian, R. Subnuclear segregation of genes and core promoter factors in myogenesis. *Genes Dev* **25**, 569-580, doi:10.1101/gad.2021411 (2011).

48 Kim, D. *et al.* TopHat2: accurate alignment of transcriptomes in the presence of insertions, deletions and gene fusions. *Genome Biol* **14**, R36, doi:10.1186/gb-2013-14-4-r36 (2013).

49 Trapnell, C. *et al.* Transcript assembly and quantification by RNA-Seq reveals unannotated transcripts and isoform switching during cell differentiation. *Nat Biotechnol* **28**, 511-515, doi:10.1038/nbt.1621 (2010).

50 Trapnell, C. *et al.* Differential analysis of gene regulation at transcript resolution with RNA-seq. *Nat Biotechnol* **31**, 46-53, doi:10.1038/nbt.2450 (2013).

51 Huang, d. W., Sherman, B. T. & Lempicki, R. A. Bioinformatics enrichment tools: paths toward the comprehensive functional analysis of large gene lists. *Nucleic Acids Res* **37**, 1-13, doi:10.1093/nar/gkn923 (2009).

52 Li, H. & Durbin, R. Fast and accurate short read alignment with Burrows-Wheeler transform. *Bioinformatics* **25**, 1754-1760, doi:10.1093/bioinformatics/btp324 (2009).

53 Landt, S. G. *et al.* ChIP-seq guidelines and practices of the ENCODE and modENCODE consortia. *Genome Res* **22**, 1813-1831, doi:10.1101/gr.136184.111 (2012).

54 Zhang, Y. *et al.* Model-based analysis of ChIP-Seq (MACS). *Genome Biol* **9**, R137, doi:10.1186/gb-2008-9-9-r137 (2008).

55 Stark, R. & Brown, G. http://bioconductor.org/packages/release/bioc/vignettes/DiffBind/inst/doc/DiffBind.pdf, 2011.

56 Zhu, L. J. *et al.* ChIPpeakAnno: a Bioconductor package to annotate ChIP-seq and ChIP-chip data. *BMC Bioinformatics* **11**, 237, doi:10.1186/1471-2105-11-237 (2010).